



HAL
open science

The dynamics of the outer edge of Saturn's A ring perturbed by the satellites Janus and Epimetheus

N Araujo, S Renner, N Cooper, M El moutamid, C Murray, B Sicardy, E
Vieira neto

► **To cite this version:**

N Araujo, S Renner, N Cooper, M El moutamid, C Murray, et al.. The dynamics of the outer edge of Saturn's A ring perturbed by the satellites Janus and Epimetheus. *Monthly Notices of the Royal Astronomical Society*, 2019, 486 (4), pp.5037-5045. 10.1093/mnras/stz1157 . hal-03105691

HAL Id: hal-03105691

<https://hal.science/hal-03105691>

Submitted on 29 May 2023

HAL is a multi-disciplinary open access archive for the deposit and dissemination of scientific research documents, whether they are published or not. The documents may come from teaching and research institutions in France or abroad, or from public or private research centers.

L'archive ouverte pluridisciplinaire **HAL**, est destinée au dépôt et à la diffusion de documents scientifiques de niveau recherche, publiés ou non, émanant des établissements d'enseignement et de recherche français ou étrangers, des laboratoires publics ou privés.

The dynamics of the outer edge of Saturn's A ring perturbed by the satellites Janus and Epimetheus

N. C. S. Araujo,¹ S. Renner²,^{2★} N. J. Cooper³,³ M. El Moutamid,⁴ C. D. Murray,³
B. Sicardy⁵ and E. Vieira Neto¹

¹Departamento de Matemática, São Paulo State University (UNESP), Campus Guaratinguetá, 12516-410 Guaratinguetá, São Paulo, Brazil

²IMCCE, Observatoire de Paris, CNRS UMR 8028, Université de Lille, Observatoire de Lille, 1 impasse de l'Observatoire, F-59000 Lille, France

³Astronomy Unit, School of Physics and Astronomy, Queen Mary University of London, Mile End Road, London E1 4NS, UK

⁴Center for Astrophysics and Planetary Science, Carl Sagan Institute, Cornell University, Ithaca, NY 14853, USA

⁵LESIA, Observatoire de Paris, Université PSL, CNRS, Sorbonne Université, Université Paris Diderot, Sorbonne Paris Cité, 5 place Jules Janssen, F-92195 Meudon, France

Accepted 2019 April 24. Received 2019 April 24; in original form 2018 October 11

ABSTRACT

We present an analytical model to study the dynamics of the outer edge of Saturn's A ring. The latter is influenced by 7:6 mean motion resonances with Janus and Epimetheus. Because of the horseshoe motion of the two co-orbital moons, the ring edge particles are alternately trapped in a corotation eccentricity resonance (CER) or a Lindblad eccentricity resonance (LER). However, the resonance oscillation periods are longer than the 4-year interval between the switches in the orbits of Janus and Epimetheus. Averaged equations of motion are used, and our model is numerically integrated to describe the effects of the periodic sweeping of the 7:6 CERs and LERs over the ring edge region. We show that four radial zones (ranges 136 715–136 723, 136 738–136 749, 136 756–136 768, and 136 783–136 791 km) are chaotic on decadal time-scales, within which particle semimajor axes have periodic changes due to partial libration motions around the CER fixed points. After a few decades, the maximum variation of semimajor axis is about 11 km (respectively 3 km) in the case of the CER with Janus (respectively Epimetheus). Similarly, particle eccentricities have partial oscillations forced by the LERs every 4 yr. For initially circular orbits, the maximum eccentricity reached is ~ 0.001 . We apply our work to 'Peggy', an object recently discovered at the ring edge, confirming that it is strongly perturbed by the Janus 7:6 LER. The CER has currently no effect on that body, nevertheless the fitted semimajor axes are just outside the chaotic zone of radial range 136 756–136 768 km.

Key words: celestial mechanics – planets and satellites: dynamical evolution and stability – planets and satellites: individual: Epimetheus – planets and satellites: individual: Janus – planets and satellites: rings.

1 INTRODUCTION

The first resolved images of the inner satellites of Saturn Janus and Epimetheus were provided in 1980 by the *Voyager 1* spacecraft (Smith et al. 1981). Small differences in the mean motions of Janus and Epimetheus (Table 1) cause the two co-orbital satellites to approach one another at intervals of about 4.2 yr. At these times, the mutual perturbations lead to a switch in their orbital configuration. In fact, in a reference frame centred on Saturn and rotating with the average mean motion, Janus and Epimetheus each follows a

horseshoe orbit separated by 180° in longitude (Yoder et al. 1983; Murray & Dermott 1999). Porco et al. (1984) examined the outer edge of Saturn's A ring using the *Voyager* data. They showed that this structure is influenced by a 7:6 inner Lindblad eccentricity resonance (LER) with the co-orbital moons (Fig. 1), the resonance forcing a seven-lobed radial distortion of amplitude 6.7 ± 1.5 km on ring particles that revolve with the average mean motion of the co-orbital satellite system. Spitale & Porco (2009) revisited the shape and kinematics of the ring edge using high-resolution (1–10 km pixel-scale) *Cassini* Imaging Science Subsystem (ISS) images spanning nearly 4 yr between 2005 and 2009, allowing the variation with time to be measured. They found that the ring edge is irregular for data obtained within about 8 months of the encounter

* E-mail: stefan.renner@univ-lille.fr

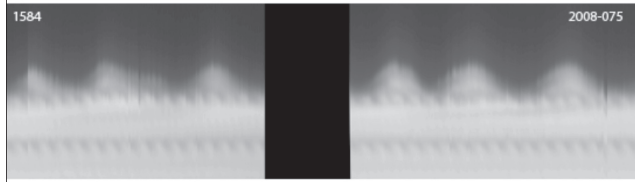


Figure 1. Mosaic of the A ring edge dominated by a seven-lobed pattern, as a result of the 7:6 inner LER with Janus (note that one lobe is not seen due to a gap in the data). The horizontal scale (corotating longitude) is from 0° to 360° and the vertical scale (radial distance) is from 136 600 to 136 900 km. The individual images (267 frames from *Cassini*'s Narrow Angle Camera on 2008 March 15) were reprojected and then assembled using a corotating frame moving at Janus' mean motion ($518:346 \text{ d}^{-1}$). The high frequency black and white patterns are due to the 35:34 and 34:33 inner LERs with Prometheus.

Table 1. Mean motions and orbital periods for Janus, Epimetheus (Cooper et al. 2015), and the outer edge of the A ring (El Moutamid et al. 2016).

	Mean motion ($^\circ \text{ d}^{-1}$)	Orbital period (d)
A ring edge	604.22	0.59581
Janus	518.35 or 518.24	0.69451 or 0.69466
Epimetheus	518.10 or 518.49	0.69484 or 0.69432

between Janus and Epimetheus that occurred in 2006, suggesting that a period of adjustment occurs as the satellites approach and recede from each switch in their orbits. Outside that adjustment period, when Janus is in the inner position of its orbit, the ring is dominated by a $m = 7$ pattern revolving at the same rate as Janus' mean motion. However, the alignment is opposite in phase to that predicted for isolated test particles: Porco & Nicholson (1987) predict that streamlines exterior to the resonance like those at the A ring edge should have one apocentre oriented towards the satellite, instead of one pericentre as observed. This configuration, also seen at the outer edge of the B ring, is most likely the result of ring-particle interactions (Porco et al. 1984). Finally, the amplitude of the radial distortion varies with time, a behaviour that Spitale & Porco (2009) attributed to a beat pattern between the perturbations from the two satellites. El Moutamid et al. (2016) extended the ring edge analysis using *Cassini* images and occultation data over a period of 8 yr from 2006 to 2014. Their fits confirmed that, for the period between 2006 and 2010 when Janus is on the inner leg of the horseshoe orbit, the A ring outer edge is dominated by the Janus 7:6 LER. However, the seven-lobed pattern disappears after the Janus/Epimetheus orbit swap in 2010 that moves the Janus resonance away from the ring edge. Moreover, El Moutamid et al. (2016) found a variety of pattern speeds with different azimuthal wave numbers, probably representing waves trapped in resonant cavities, and also identified some other signatures consistent with tesseral resonances that could be associated with inhomogeneities in Saturn's interior.

Recently, Murray et al. (2014) discovered an embedded, sub-km-radius object (nicknamed 'Peggy') at the ring edge in *Cassini* images producing localized, time-varying structures due to its gravitational perturbation of nearby ring material. The observational signature of this object has been tracked since its discovery in 2013, the deduced semimajor axis varying within ~ 10 km of the ring edge location, between 136 766 and 136 775 km. The careful tracking of the features detected leads to longitude patterns that are consistent

with the orbital evolution of several (at least two) objects. Semimajor axis changes could mainly arise from collisions with the local ring material due to the differences in relative eccentricity. Such collisions could also cause the destruction of an outwardly evolving object due to ring torques. This may explain the unusual brightness of the object seen in the discovery image by Murray et al. (2014) and the apparent disappearance of another feature soon afterwards. Moreover, the periodic sweeping of the Janus/Epimetheus 7:6 resonances may also have an effect over the orbit of the embedded object.

This is the core of this paper: predicting the consequences of the abrupt satellite semimajor axis changes at 4-yr intervals over the resonant orbits of the A ring edge particles. In fact, the strongest resonances from Janus/Epimetheus that affect the A ring edge are the corotation eccentricity resonance (CER) and the Lindblad eccentricity resonance (LER). These two types of resonances involve the following arguments: $\Psi_C = (m + 1)\lambda_S - m\lambda - \varpi_S$ and $\Psi_L = (m + 1)\lambda_S - m\lambda - \varpi$, where λ represents the geometric mean longitude, ϖ the geometric longitude of pericentre, the subscript S stands for the perturbing satellite, and $m = 6$ in the case of the ring edge. The LERs and CERs produce different effects: a CER affects the semimajor axis of the particles, forcing a libration motion inside the so-called corotation sites, but keeps orbital eccentricities almost constant. In contrast, a LER modifies eccentricities and keeps semimajor axes almost constant (El Moutamid, Sicardy & Renner 2014).

We focus on providing a short-term dynamical study of the motion of the A ring edge perturbed by the 7:6 CER/LER due to Janus and Epimetheus. Therefore the ring physical effects (collisions, viscosity, self-gravity, etc.) will not be addressed here. In particular, the goal is to understand the additional effect of the periodic trapping into the CERs, which was not considered in previous work. The paper is organized as follows. Section 2 summarizes the orbital characteristics of Janus–Epimetheus and gives an overview of the CERs/LERs affecting the edge of the A ring. Section 3 presents the analytical modelling, basically averaged equations of motion near the resonances and associated time-scales. Numerical simulation results are examined and the model is applied to object 'Peggy' in Section 4. Concluding remarks are given in Section 5.

2 MOTION OF JANUS–EPIMETHEUS AND RESONANCES AT THE A RING EDGE

Fig. 2 shows the time evolution of the semimajor axes and the switches in the orbits of Janus and Epimetheus, resulting from a numerical model fitted to *Cassini* ISS astrometric data for all the inner satellites (Cooper et al. 2015). For this fit, the state vectors and masses were solved at the epoch 2007 June 1 00:00:00.0, and ephemerides spanning the period 2000–2020 were generated. As a result, Table 2 gives the geometric orbital elements for Janus and Epimetheus computed from the state vectors using the method of Renner & Sicardy (2006), and the parameters of Saturn given in Table 3.

The radial widths of the librational arcs of Janus and Epimetheus in Fig. 2 have a ratio equal to the mass ratio (~ 3.6 , see Table 2), as a consequence of the conservation of angular momentum. Thus, Janus has the smaller variations in semimajor axis since it is the more massive moon. The difference between the semimajor axes of the two satellites is approximately 48 km. Note that away from the approaches, the radial separation between the satellites is not constant: it is maximum for a relative longitude corresponding to

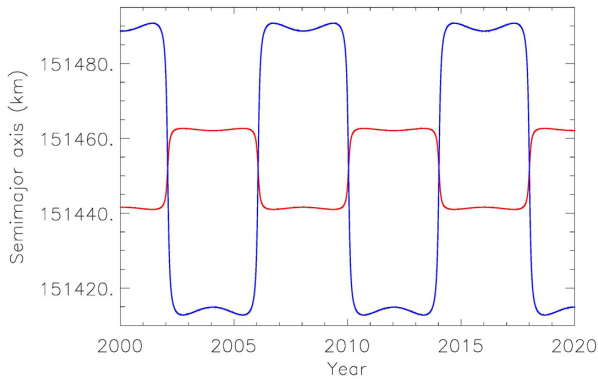


Figure 2. Semimajor axis for Janus (red) and Epimetheus (blue) as a function of time between 2000 and 2020, from a numerical integration fitted to *Cassini* data (Cooper et al. 2015). The initial conditions and Saturn’s parameters are given in Tables 2 and 3, respectively.

Table 2. Geometric orbital elements for Janus and Epimetheus at epoch 2007 June 1 00:00:00.0 UTC (JED 245 4252.50075446), computed from fits to *Cassini* observations (Cooper et al. 2015). At this epoch, the orbit of Janus is in the inner position.

	Janus	Epimetheus
Mass (kg)	1.896×10^{18}	5.262×10^{17}
a (km)	151441.171	151488.969
e	0.00677	0.00972
i (°)	0.16446	0.35199
Ω (°)	16.03786	53.92315
ϖ (°)	328.67973	79.18426
λ (°)	268.22574	145.38974

Note. The elements a , e , i , Ω , ϖ , and λ are, respectively, the semimajor axis, the eccentricity, the inclination, the longitude of ascending node, the longitude of pericentre, and the mean longitude. Mean motion and the pericentre precession rates are derived self-consistently from the semimajor axis using the Saturn constants given in Table 3.

Table 3. Saturn constants, from Cooper et al. (2015).

Constant	Value	Units
GM	$3.793120706585872 \times 10^7$	$\text{km}^3 \text{s}^{-2}$
Radius	60330	km
J_2	$1.629084747205768 \times 10^{-2}$	
J_4	$-9.336977208718450 \times 10^{-4}$	
J_6	$9.643662444877887 \times 10^{-5}$	

the L_4 , L_5 Lagrangian points, and minimum at the longitude of the L_3 point (Dermott & Murray 1981a,b).

The direct consequence of the horseshoe motion is that the locations of the 7:6 resonances by Janus–Epimetheus shift inwards or outwards every 4 yr. Since the semimajor axis difference between the resonances is comparable to the radial excursions of the two satellites, the particles located in three specific regions (around semimajor axes $\sim 136\,740$, $136\,765$, and $136\,785$ km) are alternately trapped in a CER or a LER. This peculiarity is presented in Fig. 3 and Table 4, which give the resonance locations and widths. For instance, when Janus is in the outer position, the ring edge is roughly at Janus CER position, with the (weaker) Epimetheus LER located inside the ring and the (stronger) Janus one displaced outside,

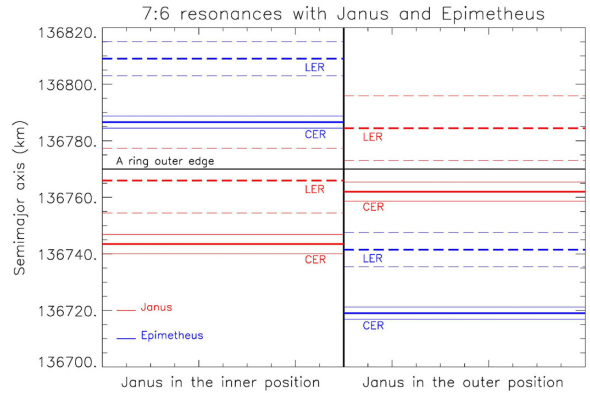


Figure 3. Semimajor axes of the 7:6 resonances with Janus (in red) and Epimetheus (in blue) at the edge of the A ring (solid black line representing its average location; see El Moutamid et al. 2016). The LERs and CERs appear, respectively, as thick dotted and solid lines, when Janus is in the inner position on the left, or in the outer position on the right. The full widths of the resonances are indicated by thinner lines on either side of the resonance position. See Table 4 and text for details.

Table 4. Numerical values (km) for the locations of the 7:6 resonances shown in Fig. 3. The full widths are in parentheses and are given by equations (4) and (7). The locations of the resonances are computed iteratively by cancelling the time derivatives of the resonance angles, and using the mean motion values, the pericentre precession rates from Table 1 and 2, and the Saturn parameters given in Table 3.

	Janus inside	Janus outside
LER	136 809.1 (12.1)	136 784.5 (22.9)
CER	136 786.6 (4.3)	136 762.0 (6.8)
LER	136 765.9 (22.9)	136 741.5 (12.1)
CER	136 743.5 (6.8)	136 719.0 (4.3)

thus explaining the smaller eccentricities of the ring edge fitted by Spitale & Porco (2009) for observations a few months preceding the inward swap of Janus. As demonstrated in Sections 3 and 4, the CERs also cause significant perturbations on the ring particles, in spite of the low-eccentricity orbits of Janus and Epimetheus.

Fig. 4 shows two *Cassini* ISS high-resolution images of the A ring edge where the locations of the relevant 7:6 resonances have been superimposed, one corresponding to Janus in the inner position and the other in the outer position. Thanks to a grazing illumination, these data clearly reveal the presence of clumps with vertical extents. By selecting another longitude interval to produce the top image, note that the ring edge would instead match the location of the LER with Janus. Indeed the edge is structured by seven lobes of radial amplitude ~ 15 km (Spitale & Porco 2009), a distance comparable to the location difference between the CER with Epimetheus and the LER with Janus.

We can neglect the inclination of Janus and Epimetheus in this work. Indeed, the mean motion inclination resonances are located well inside the edge of the A ring. The strongest of these resonances are, respectively, the corotation inclination resonance (CIR) and the Lindblad inclination resonance (LIR), for which the critical angles are $\Psi_{\text{CIR}} = 2[(m+1)\lambda_S - m\lambda - \Omega_S]$ and $\Psi_{\text{LIR}} = 2[(m+1)\lambda_S - m\lambda - \Omega]$. When Janus is in the inner position, the nearest resonance to the ring edge is the CIR due to Epimetheus located at a semimajor axis of 136 684 km. When Janus is in the outer position, the nearest one is the CIR due to Janus at 136 660 km.

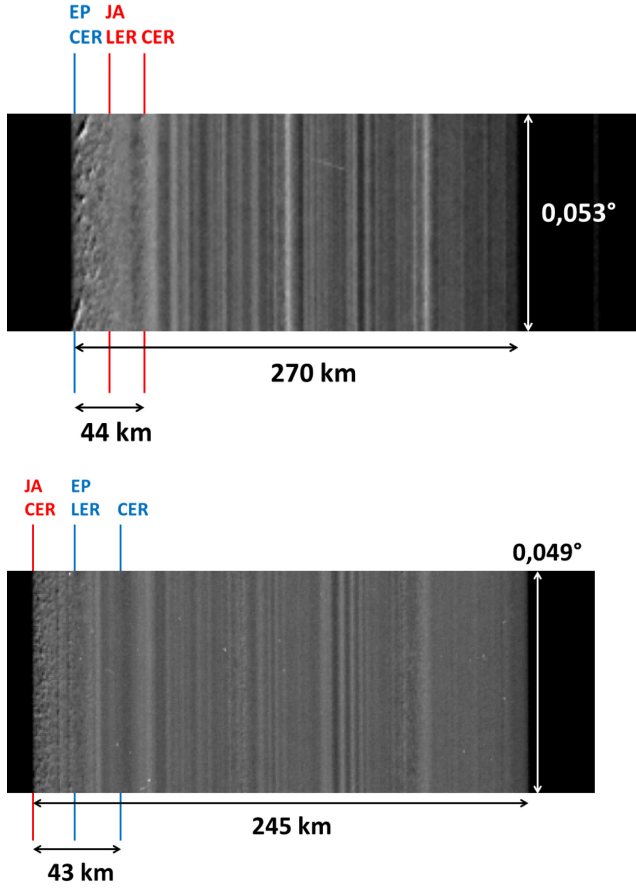


Figure 4. *Cassini* ISS high-resolution images showing narrow parts of the A ring edge. The top image was cropped from the *Cassini* frame N1591063789_1, ISS_070RI.PAZSCN001.PRIME, 2008-154T01:30:09.718Z, and the bottom one from N1656998640.1, ISS_134DA.DAPHNIS001.VIMS, 2010-186T04:38:30.079Z. The locations of the 7:6 resonances have been superimposed. Janus is in the inner (respectively outer) position at the epoch of the top (respectively bottom) image. The black part on the right is the Keeler gap.

3 AVERAGED EQUATIONS OF MOTION

Near a CER, the average motion of a test particle can be described by the following two variables:

$$\xi = \frac{a - a_C}{a},$$

$$\psi_C = (m + 1)\lambda_S - m\lambda - \varpi_S,$$

where a_C is the CER radius, ξ is the non-dimensional distance from the exact CER, m is a positive (respectively negative) integer when the particle's orbit is inside (respectively outside) that of the satellite, and ψ_C is the CER critical angle.

The motion near a LER is depicted by the eccentricity vector (h , k) of the particle:

$$h = e \cos(\psi_L),$$

$$k = e \sin(\psi_L),$$

where the LER argument $\psi_L = (m + 1)\lambda_S - m\lambda - \varpi$ measures the difference between the longitude of conjunction with the satellite and the pericentre longitude of the particle.

The method to compute the rates of change of ξ , ψ_C , h , and k is detailed in Araujo (2017), based on previous work by e.g. Shu (1984), Sicardy (1991), and Foryta & Sicardy (1996). The classical technique is to expand the perturbing potential near the first-order

$m + 1$: m resonance, taking into account the secular terms due to the central planet's oblateness and ignoring the rapidly varying angles, and then to derive the time variation of the orbital elements from the total averaged Hamiltonian. The resulting equations of motion can be written as

$$\begin{cases} \dot{\xi} = -2mn \frac{M_S}{M} \frac{a}{a_S} E e_S \sin(\psi_C), \\ \dot{\psi}_C = \frac{3}{2} mn \xi, \\ \dot{h} = -(\Delta n)k, \\ \dot{k} = +(\Delta n)h + \frac{a}{a_S} \frac{M_S}{M} n A. \end{cases} \quad (1)$$

The first two equations of the system (1) describe the CER and the last two describe the LER, where n is the mean motion, M_S (respectively M) is the mass of the perturbing satellite (respectively the planet), and $\Delta n = \psi_L \simeq (m + 1)n_S - mn$ ($\dot{\varpi} \ll n$) is the distance in frequency from the exact LER. The coefficients E and A are combinations of Laplace coefficients b_ν^m (Shu 1984):

$$E = -\frac{1}{2} [(2m + 1) + \alpha D] b_{1/2}^m(\alpha) \simeq -0.802m,$$

$$A = \frac{1}{2} [2(m + 1) + \alpha D] b_{1/2}^{m+1}(\alpha) \simeq 0.802m,$$

where $\alpha = \frac{a}{a_S}$, $D = \frac{d}{d\alpha}$ and where the approximations hold for large $|m|$.

We apply the model above by numerically integrating the system (1) with $m = 6$, Saturn as central body, Janus or Epimetheus as perturbing satellite, and by changing semimajor axes for Janus/Epimetheus every 4.2 yr, which alternately traps particles in a CER (first two equations of system 1) or a LER (last two equations). This allows us to study in a simple and satisfactory way the dynamics of the ring edge, as confirmed by comparative full N -body simulations (Section 4). Note that equation (1) does not contain any coupling between the CER and LER as discussed in El Moutamid et al. (2014), since the two types of resonances are sufficiently isolated in the case of the A ring edge (Fig. 3).

The two CER equations of the system (1) reduce to the simple pendulum equation:

$$\ddot{\psi}_C = -3m^2 n^2 \frac{M_S}{M} \frac{a}{a_S} E e_S \sin(\psi_C). \quad (2)$$

This equation has the following integral of motion:

$$J = -\frac{3}{8} \xi^2 + \frac{M_S}{M} \frac{a}{a_S} E e_S \cos(\psi_C), \quad (3)$$

from which we derive the full width of the corotation site,

$$W_C = \frac{8}{\sqrt{3}} a_C \sqrt{\frac{M_S}{M} \frac{a}{a_S} |E| e_S}. \quad (4)$$

This yields $W_C = 6.8$ and 4.3 km in the case of Janus and Epimetheus, respectively.

Equation (2) can be developed near the centre of the corotation site ($\psi_C = 180^\circ$, $\xi = 0$) to obtain the CER libration period:

$$P_{\text{CER}} = \frac{P_{\text{ORB}}}{|m|} \left(3 \frac{M_S}{M} \frac{a}{a_S} E e_S \right)^{-1/2}. \quad (5)$$

We find $P_{\text{CER}} = 14.5$ (Janus) and 23.0 yr (Epimetheus).

The effect of the LER is to induce a forced eccentricity on particles given by the fixed points $\dot{h} = \dot{k} = 0$ in equation (1):

$$e_f = -\frac{a}{a_s} \frac{M_s}{M} \frac{n}{\Delta n} A. \quad (6)$$

In a frame rotating with the satellite, the particle motions are $(m + 1)$ -lobed patterns called streamlines. The value of e_f decreases as the distance from the exact resonance increases, with a shift of π for the streamlines on opposite sides of the resonance. The width of the LER is determined by the distance from the resonance such that the value of the forced eccentricity is large enough to intersect an outer streamline with an inner one (Porco & Nicholson 1987; Murray & Dermott 1999). Then a good approximation for the width of the influence of the LER is given by

$$W_{\text{LER}} = 2.9a \sqrt{\frac{M_s}{M}}, \quad (7)$$

i.e. 22.9 and 12.1 km in the case of Janus and Epimetheus, respectively.

From equation (1), the oscillation period of the eccentricity vector (h, k) is

$$P_{\text{LER}} = \frac{2\pi}{|\Delta n|}. \quad (8)$$

For example with $a = 136\,770$ km and when Janus is in the inner position, $P_{\text{LER}} = 6.0$ yr. Therefore, the CER and LER libration periods are greater than the 4-yr period of orbital swap between Janus and Epimetheus.

4 NUMERICAL SIMULATION

Ring edge particle motions are numerically integrated from the model presented in the previous section. These simulations are also compared to full N -body integrations. The full equations of motion are integrated in a Saturn-centred Cartesian reference frame, using Everhart’s 15th-order Radau algorithm (Everhart 1985) and taking into account the effects of the planet’s oblateness up to and including terms in J_6 . State vectors are converted into geometric orbital elements using the algorithm given by Renner & Sicardy (2006). Indeed, these elements are not contaminated by the short-period terms caused by planetary oblateness, contrary to the classical osculating elements. Except Janus and Epimetheus, the perturbations from the other Saturnian satellites are neglected. Here we summarize the results.

4.1 Individual particle behaviour

Fig. 5 typically illustrates the dynamical response of a test particle alternately perturbed by the CER/LER due to Janus–Epimetheus. Initially, the particle has no eccentricity and a semimajor axis $a = 136\,757.5$ km, corresponding to the radial zone perturbed by the Janus resonances only, see Fig. 3.

Because of the horseshoe motion, the location of the 7:6 CER shifts from $a = 136\,743.5$ to $136\,762.0$ km (Table 4) every 4.2 yr, periodically trapping the test particle in this resonance of full width 6.8 km. Since the libration period (14.5 yr near the CER fixed point) is longer than the interval between the orbital switches, the particle does not complete the full libration cycle. The particles instead enter corotation sites with random phases, which randomly increase or decrease their semimajor axes as a result of the partial CER libration motion. Consequently the motion is chaotic, as shown in the next section (Fig. 7): starting with two sets of very close initial conditions

can lead to very different final positions after a few passages into resonance. Nevertheless, the semimajor axis range explored by the particle is of the same order as the CER full width. When Janus is in the inner position, the CER is at $a = 136\,743.5$ km well inside the ring particle’s orbit, leaving its semimajor axis constant at first order. In that case the LER location ($a = 136\,766$ km) and the particle’s orbit are close, exciting the eccentricity (top right-hand plot of Fig. 5). Again, the LER libration period (6 yr for a particle’s semimajor axis $a = 136\,770$ km) is longer than the interval between the orbital switches. After a few trappings in the LER, the eccentricity grows up to $\sim 10^{-3}$, a value in good agreement with the analytical estimate (equation 9). When Janus is in the outer position, the particle’s eccentricity remains almost constant as the LER moves 20 km outwards.

The middle and bottom plots of Fig. 5 show that the particle remains trapped into resonance (CER or LER) when we arbitrarily remove Epimetheus from the simulation at different times, thus cancelling the orbital switches between the two co-orbital moons. With Epimetheus removed at $t = 43.5$ yr corresponding to Janus in the outer position, the 7:6 CER argument librates and the semimajor axis oscillates around the CER radius, with an amplitude and a period that compare well with the formulas (4) and (5), respectively. Similarly, the LER argument and the particle’s eccentricity oscillate when Epimetheus is removed at $t = 64.3$ yr corresponding to Janus in the inner position, with a period given by equation (8).

4.2 Cumulative effects

In order to assess the overall effect of the resonances on the ring edge, we consider 10 000 test particles with initial semimajor axes uniformly distributed with a spacing of 0.5 km between 136 700 and 136 820 km, where the 7:6 resonances are located (Fig. 3). Initial mean longitudes are also uniformly distributed and eccentricities are fixed at zero. For each given semimajor axis value, the motion of 10 particles is integrated with an integration time of 500 yr, corresponding to several dozens of librational paths of Janus–Epimetheus. The initial conditions for Janus and Epimetheus are given in Table 2. We compute the maximum variation of semimajor axis for ring edge test particles, defined as the difference between the largest and the smallest semimajor axis value reached during the simulation. The results are shown in Fig. 6. Four radial zones centred on the CER radii (Table 4) exhibit large semimajor axis variations. These changes in semimajor axis result from the periodic but partial libration motions around the CER fixed points (Fig. 5 top left). The semimajor axis intervals of the four regions are: 136 715–136 723, 136 738–136 749, 136 756–136 768, and 136 783–136 791 km. The maximum variations reached are, respectively, ~ 11 and 3.5 km for particles perturbed by Janus and Epimetheus CERs. The values are larger in the case of the Janus since the latter has a larger mass, and are of the same order as the CER full widths (Table 4). Modulations of semimajor axis for particles located near but outside the resonance (circulation) and/or the CER sweeping every 4.2 yr may explain why the radial zones can be larger than the CER full width, as is the case for Janus CER.

Since particles get into the CERs with random phases, motions in the four radial zones of Fig. 6 are chaotic. We demonstrate the chaoticity using the fast Lyapunov indicator (FLI) method (Froeschlé, Gonczi & Lega 1997; Froeschlé & Lega 2000). To compute the FLI time evolution, the variational equations are integrated simultaneously with the full equations of motion, still taking into account the effects of Saturn’s oblateness (up to J_6 included) and using the same physical parameters of Saturn, masses

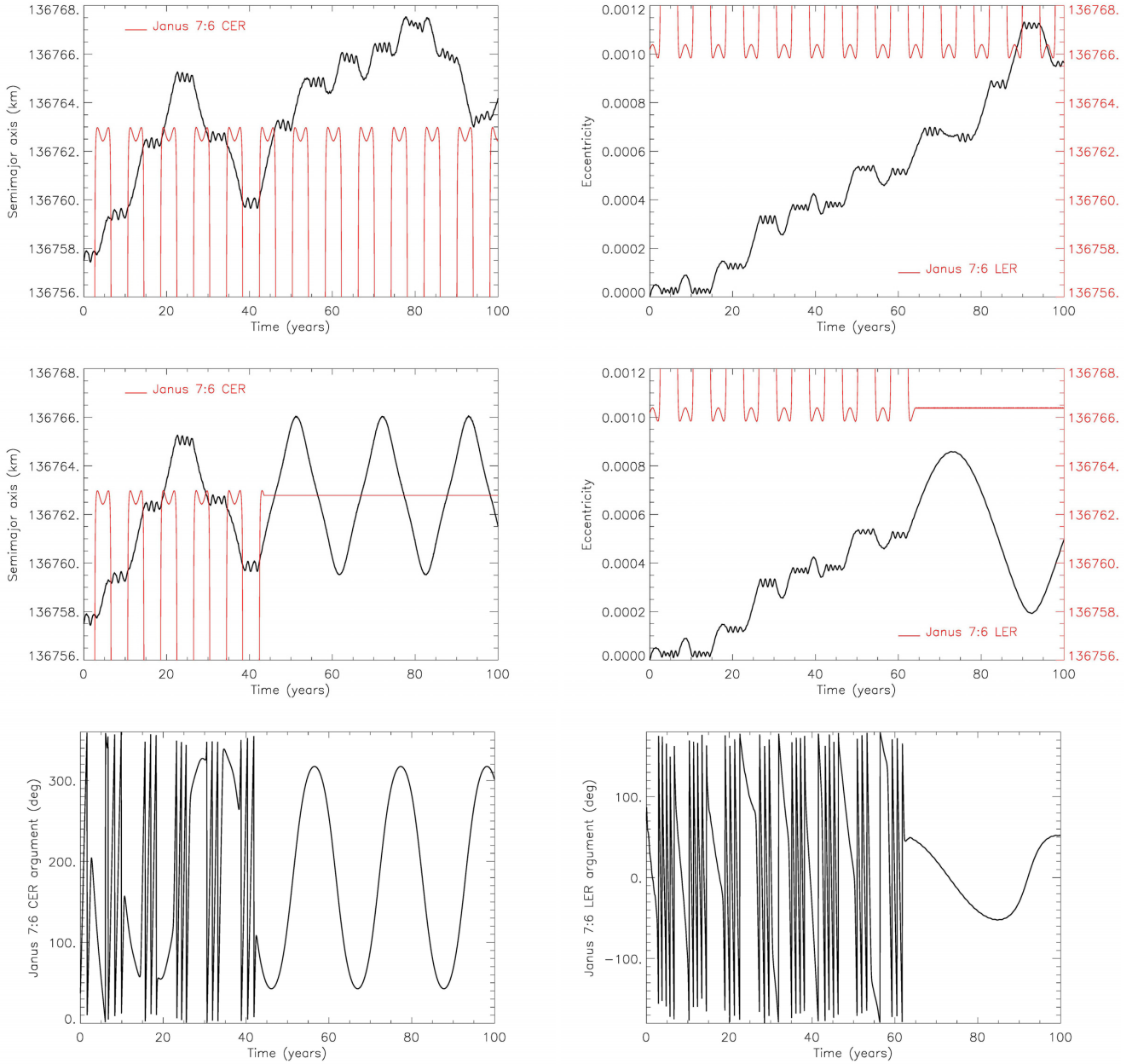


Figure 5. Time evolution of a ring edge test particle, alternately trapped in the 7:6 Janus CER and then in the 7:6 Janus LER. Top left: semimajor axis (black) and location of the 7:6 CER (red). Top right: eccentricity (black) and location of the 7:6 LER (red). Middle left: semimajor axis (black) and location of the 7:6 CER (red), with Epimetheus removed from the simulation at $t = 43.5$ yr. Middle right: eccentricity, with Epimetheus removed from the simulation at $t = 64.3$ yr. Bottom left: 7:6 CER argument, with Epimetheus removed from the simulation at $t = 43.5$ yr. Bottom right: 7:6 LER argument, with Epimetheus removed from the simulation at $t = 64.3$ yr.

and initial states for Janus/Epimetheus (Table 3 and 2, respectively). Some details on the method are given in e.g. Cooper et al. (2015). For a given autonomous dynamical system $\dot{\mathbf{x}} = \mathbf{f}(\mathbf{x})$, the FLI is defined by $\text{FLI} = \sup_{0 < t < t_f} \ln \|\mathbf{w}(t)\|$, where \mathbf{w} is a deviation/tangent

vector solution of the variational equations $\dot{\mathbf{w}} = \frac{\partial \mathbf{f}}{\partial \mathbf{x}}(\mathbf{x})\mathbf{w}$ of the system. The FLI is in fact the initial part, up to a stopping time t_f , of the computation of the maximum Lyapunov characteristic exponent, making it a faster tool to distinguish chaotic from regular orbits. For a chaotic orbit, the FLI grows linearly with time, whereas the FLI

of a regular orbit has a logarithmic growth. The inverse of the FLI slope defines the Lyapunov time, the characteristic time-scale that measures the time needed for nearby orbits of the system to diverge by e . Typical results are presented in Fig. 7. The three upper curves are chaotic orbits for particles of the three outer radial zones of Fig. 6 that exhibit large variations of semimajor axes. The slopes of the FLI evolution correspond to Lyapunov times of 10–15 yr, meaning that just a few CER encounters are sufficient to make neighbouring orbits diverge.

Fig. 8 shows the maximum eccentricity of ring edge particles (initially on circular orbits), using the same method applied for the

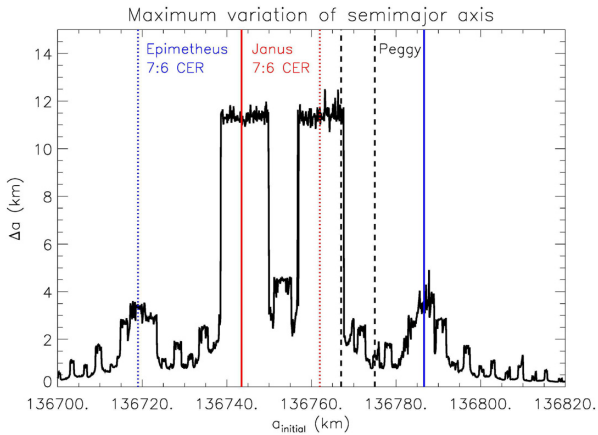


Figure 6. Maximum variation of semimajor axis for ring edge test particles. The initial semimajor axes are uniformly distributed between 136 700 and 136 820 km, with a spacing of 0.5 km. For each given semimajor axis value, the motion of 10 particles is integrated, varying the initial mean longitude uniformly along the orbit. The particle that experiences the largest variation of semimajor axis is identified. This variation is defined as the difference between the largest and the smallest semimajor axis value reached during the simulation. The integration time is 500 yr, corresponding to several dozens of librational paths of Janus–Epimetheus. The locations of the 7:6 CER are indicated in red (Janus) and blue (Epimetheus). The solid (respectively dotted) lines correspond to Janus in the inner (respectively outer) position. The black dashed lines represent the range of semimajor axes determined for Peggy (Cooper & Murray, private communication).

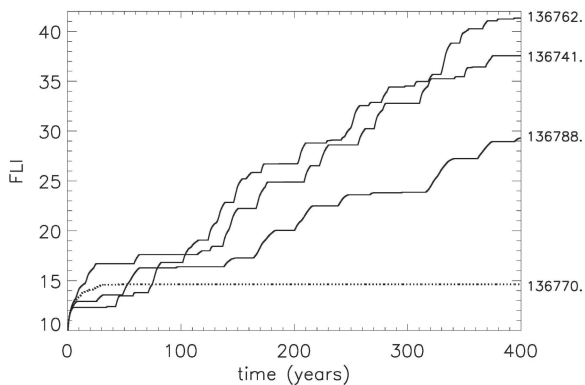


Figure 7. FLI versus time for particles at Saturn’s A ring edge. The three upper curves represent chaotic orbits for particles of the three outer radial zones of Fig. 6 (initial semimajor axes 136 788, 136 741, and 136 762 km, respectively). The lower dotted curve shows a regular behaviour for a particle at 136 770 km, i.e. the typical value defining the ring edge.

maximum changes in semimajor axis. Eccentricities reach values up to 10^{-3} for particles at the locations of the 7:6 LER. This is consistent with the analytical expression obtained from classical resonance theory for initially circular orbits (Henrard & Lemaître 1983; Malhotra 1998):

$$e_{\text{MAX}} = 2 \left| \frac{4}{3} \frac{a}{a_S} \frac{A}{m^2} \frac{M_S}{M} \right|^{1/3}, \quad (9)$$

which yields 1.7×10^{-3} (respectively 1.1×10^{-3}) in the case of Janus (respectively Epimetheus).

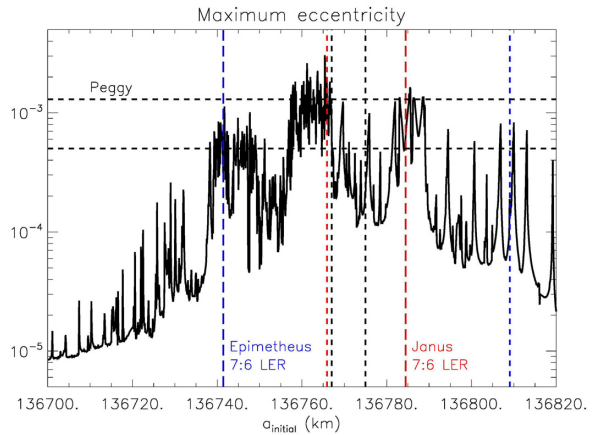


Figure 8. Maximum eccentricity for ring edge test particles. The same method as to derive the maximum change in semimajor axis (Fig. 6) is used. The integration time is 500 yr. The locations of the 7:6 LER are indicated in red (Janus) and blue (Epimetheus). The black dashed lines represent the range of semimajor axes and eccentricities determined for Peggy (Cooper & Murray, private communication).

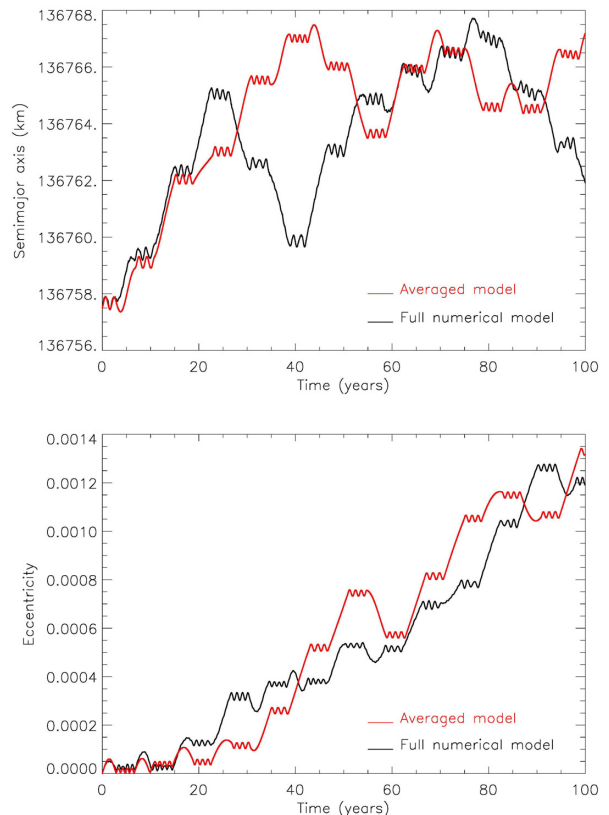


Figure 9. Semimajor axis and eccentricity time evolution for a ring edge particle. The red curve is given by the model, and the black curve is from a full numerical integration including Janus, Epimetheus, and Saturn’s oblateness up to and including terms in J_6 .

A comparison of the orbital elements (semimajor axis and eccentricity) as a function of time for ring edge particles is displayed Fig. 9. These elements are derived from both the analytical model (red) and a four-body simulation (black) including Janus,

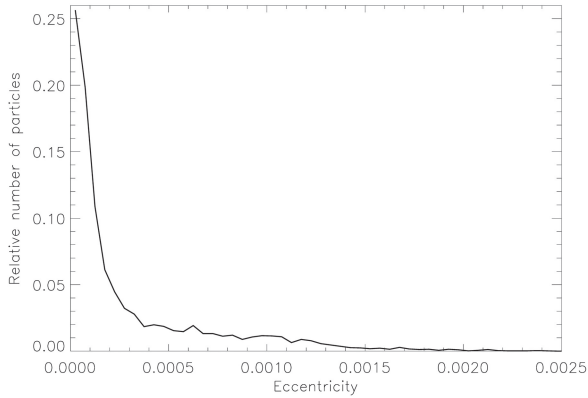


Figure 10. Distribution of particle eccentricities in the ring edge region from a 500 yr simulation. The initial semimajor axes are uniformly distributed between 136 750 and 136 800 km. Particles can reach the theoretical maximum value $\sim 10^{-3}$. Most of the particles have eccentricity values in good agreement with the observed ones (Spitale & Porco 2009; El Moutamid et al. 2016).

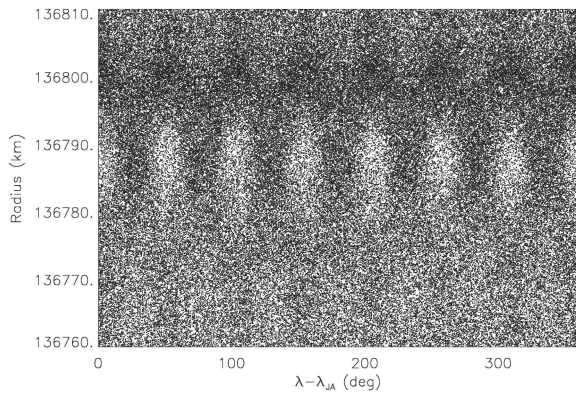


Figure 11. Orbital radii of ring edge particles versus mean longitude in a frame rotating with Janus’ mean motion. The plot shows the accumulated positions of particles on 4.2 yr, with a time step of 0.1 yr and after an integration time of 400 yr, when Janus LER is at 136 784 km (Janus in the outer position).

Epimetheus, Saturn’s oblateness (up to J_6 included), and a test particle. The integration of the averaged equations is in very good agreement with the full numerical model, confirming that the system (1) reproduces the main features of the motion. Fig. 9 also confirms the short Lyapunov times derived from the FLI computation, as very close initial orbits move away after just 2–3 CER encounters.

Particle eccentricities from the model are similar to the observed values derived from *Cassini* imaging. The histogram (Fig. 10) essentially shows values from 10^{-5} to 10^{-4} , a range comparable to the eccentricity variation among the Spitale & Porco (2009) data sets. The $m = 7$ pattern resulting from the 7:6 LER is also clearly visible in Fig. 11 that shows, as a function of mean longitude in a frame rotating with Janus’ mean motion, the orbital radii of ring edge particles accumulated over 4.2 yr (after 400 yr of integration and with a time step of 0.1 yr) when Janus LER is at 136 784 km (outer position). The amplitude ae of this pattern is about 15 km, corresponding to an eccentricity of order 10^{-4} akin to the value derived from the simultaneous fit to all data sets in Spitale & Porco

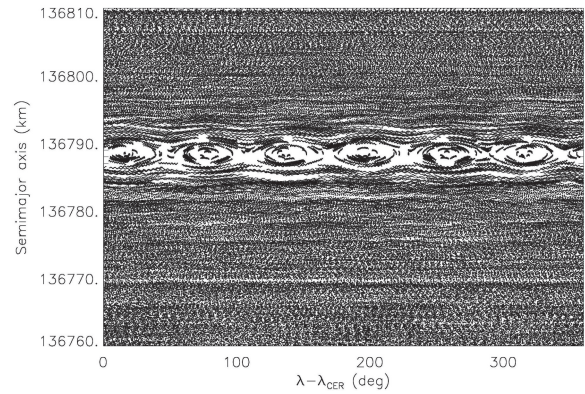


Figure 12. Semimajor axes of ring edge particles versus mean longitude in a frame rotating at pattern speed n_{CER} . The accumulated positions of particles on 4.2 yr are displayed, with a time step of 0.1 yr, when Epimetheus CER is at 136 787 km (Epimetheus in the outer position).

(2009). Note that the density of particles is lower on a wide orbital radius range between $\sim 136 740$ and 136 790 km, since a significant fraction of particles have reached higher eccentricities due to the repeated LER perturbations (Figs 8 and 10).

4.3 Application to Peggy’s orbital elements

The object Peggy is currently not perturbed by the CERs. In fact, the semimajor axis range (136 767–136 775 km, see Fig. 6) derived for that body from *Cassini* observations (Cooper & Murray, private communication) is located right next to the outer chaotic radial zone (centred at 136 762 km) due to Janus CER. On the other hand, the eccentricity interval (5×10^{-4} – 2×10^{-3}) is compatible with the maximum eccentricity forced by the LERs (Fig. 8), and matches even better the values around 136 760 km. This raises the idea that the object possibly formed in the CER region before moving outwards to its current location.

In Fig. 12, particle semimajor axes are displayed as a function of mean longitude in a frame rotating with the CER pattern speed n_{CER} , when Epimetheus CER is located at 136 787 km. The six corotation sites are distinguishable. The partial libration motions around the CER fixed points create clumpy structures along the ring. These structures, which extend over a few kilometres in the radial direction and have various longitudinal lengths up to dozens of degrees, are undetectable in *Cassini* ISS data. Fig. 13 shows an example where a test particle, randomly trapped every 4.2 yr into the 7:6 CER with Janus, moves to the outer part of the ring edge at $\sim 136 767$ km, i.e. the lowest possible semimajor axis for Peggy. It is therefore possible that the periodic trapping into CERs with Janus/Epimetheus may help to aggregate ring particles into larger objects at the ring edge.

5 CONCLUSIONS

We numerically examined an analytical model that describes the dynamics of the outer edge of Saturn’s A ring. While the seven-lobed radial distortion of the A ring edge resulting from the 7:6 Janus LER is well known (Porco et al. 1984), our work is the first study to explain the effects of periodic perturbations by CERs, arising from co-orbital satellites in horseshoe motion.

In terms of orbital elements, we find that the semimajor axis evolution is dominated by chaotic jumps due to periodic captures

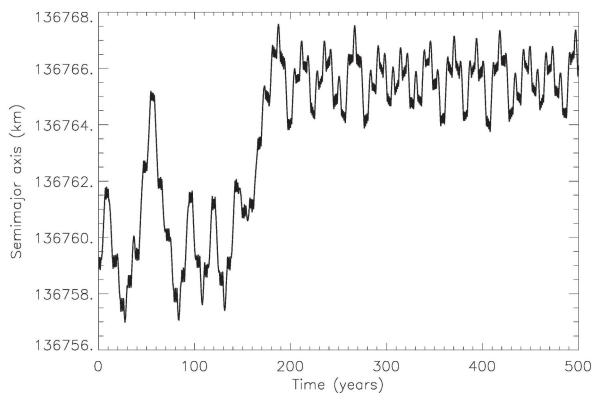


Figure 13. Semimajor axis time evolution for a test particle, driven to the outer part of the ring edge by the chaotic crossings of the 7:6 CER with Janus.

into CERs with Janus and Epimetheus. These semimajor axis variations are comparable (or slightly larger) than those expected from the oscillations into the CER sites (Fig. 6). Similarly, the eccentricity experiences step-by-step increases due to periodic LER perturbations, before eventually reaching the maximum value forced by the resonance (equation 9). A good agreement is found between the simulated and observed eccentricities of A ring edge particles (Spitale & Porco 2009; El Moutamid et al. 2016).

We showed that the object Peggy recently discovered at the ring edge (Murray et al. 2014) is strongly perturbed by the Janus 7:6 LER (when Janus is on its inner leg of its libration motion), but not currently perturbed by any CER, with fitted semimajor axes just outside one of the four chaotic radial zones (Fig. 6). The model presented suggests that the periodic CER/LER perturbations due to the co-orbital moons may help to form objects at the ring edge from particles that move outwards. This dynamical mechanism would add to (long-term) satellite formation processes such as the viscous spreading of the rings (Charnoz, Salmon & Crida 2010) or the ejection from the rings of objects denser than ice (Charnoz et al. 2011).

ACKNOWLEDGEMENTS

NCSA thanks the Coordenação de Aperfeiçoamento de Pessoal de Nível Superior – Brasil (CAPES) – Finance Code 001. NJC and CDM thank the Science and Technology Facilities Council

(Grant No. ST/P000622/1) for financial support. Part of the research leading to these results has received funding from the European Research Council under the European Community’s H2020 (2014–2020/ERC Grant Agreement No. 669416 ‘LUCKY STAR’). The authors also thank Thomas Rimlinger for useful comments, the Encelade working group for interesting discussions, the International Space Science Institute (ISSI) for support, and the members and associates of the *Cassini* ISS team.

REFERENCES

- Araujo N., 2017, PhD thesis, Universidade Estadual Paulista, Guaratinguetá
- Charnoz S., Salmon J., Crida A., 2010, *Nature*, 465, 752
- Charnoz S. et al., 2011, *Icarus*, 216, 535
- Cooper N. J., Renner S., Murray C. D., Evans M. W., 2015, *AJ*, 149, 27
- Dermott S. F., Murray C. D., 1981a, *Icarus*, 48, 1
- Dermott S. F., Murray C. D., 1981b, *Icarus*, 48, 12
- El Moutamid M., Sicardy B., Renner S., 2014, *Celest. Mech. Dyn. Astron.*, 118, 235
- El Moutamid M. et al., 2016, *Icarus*, 279, 125
- Everhart E., 1985, in Carusi A., Valsecchi G. B., eds, Proc. IAU Colloq. 83, ASSL Vol. 115, Dynamics of Comets: Their Origin and Evolution. Reidel, Dordrecht, p. 185
- Foryta D. W., Sicardy B., 1996, *Icarus*, 123, 129
- Froeschlé C., Lega E., 2000, *Celest. Mech. Dyn. Astron.*, 78, 167
- Froeschlé C., Gonczi R., Lega E., 1997, *Planet. Space Sci.*, 45, 881
- Henrad J., Lemaître A., 1983, *Celest. Mech.*, 30, 197
- Malhotra R., 1998, in Lazzaro D., Vieira Martins R., Ferraz-Mello S., Fernandez J., eds, ASP Conf. Ser. Vol. 149, Solar System Formation and Evolution. Astron. Soc. Pac., San Francisco, p. 37
- Murray C. D., Dermott S. F., 1999, Solar System Dynamics. Cambridge Univ. Press, Cambridge
- Murray C. D., Cooper N. J., Williams G. A., Attree N. O., Boyer J. S., 2014, *Icarus*, 236, 165
- Porco C. C., Nicholson P. D., 1987, *Icarus*, 72, 437
- Porco C., Danielson G. E., Goldreich P., Holberg J. B., Lane A. L., 1984, *Icarus*, 60, 17
- Renner S., Sicardy B., 2006, *Celest. Mech. Dyn. Astron.*, 94, 237
- Shu F. H., 1984, in Greenberg R., Brahic A., eds, IAU Colloq. 75, Planetary Rings. Univ. Arizona Press, Tucson, AZ, p. 513
- Sicardy B., 1991, *Icarus*, 89, 197
- Smith B. A. et al., 1981, *Science*, 212, 163
- Spitale J. N., Porco C. C., 2009, *AJ*, 138, 1520
- Yoder C. F., Colombo G., Synnott S. P., Yoder K. A., 1983, *Icarus*, 53, 431

This paper has been typeset from a $\text{\TeX}/\text{\LaTeX}$ file prepared by the author.